

A Fast Convergence Of Disturbances Using One Inductor Multi-Port Inverter For Addressing EV System

K.Sai Sucharitha^{1*}, B. Poojitha², P. G. Priyanka³, G. V. Deepika Priya⁴, R. Vamshi Chenna Keshava Reddy⁵
Aslam Shaik⁶

^{1,2,3,4,5}UG Students, EEE, Chaitanya Bharathi Institute of Technology, Proddatur
⁶Associatant Professor, EEE, Chaitanya Bharathi Institute of Technology, Proddatur
*Corresponding Author email id: ksucharitha2004@gmail.com

Abstract—In this paper, a Super-Twisting Sliding Mode Control (STSMC) system for a Single Inductor Multi-Port Power Converter (SIMPC) in electric vehicle (EV) applications is designed and implemented. By offering stable control under a range of load conditions and disturbances, the suggested STSMC technique improves power converter performance. System stability is increased and chattering is effectively decreased by the controller's super-twisting algorithm. When compared to conventional control techniques, the compensator-based system produces a smoother and more reliable operation by further reducing distortions in the output voltage and output current. Results from experiments and simulations show that the suggested STSMC system performs better in terms of improved disturbance rejection, decreased steady-state error, and quick dynamic response. Furthermore, the system shows particularly lower voltage and current distortions, increasing overall multi-port efficienc.

Index Terms—state-space modeling, Multi-port DC-DC converters, electric vehicles, hybrid energy storage system, STSMC Controller.

I. INTRODUCTION

As the world's energy demands keep growing and fossil fuels become harder to find, electric vehicles (EVs) powered by clean energy are really coming into the limelight. Solar PV systems play a critical role in this shift, especially when they use maximum power point tracking (MPPT). They also depend on hybrid energy storage systems (HESS) to keep everything running smoothly. To efficiently manage this energy, we look to multiport DC-DC converters, with the non-isolated types being especially popular due to their compact size and cost-effectiveness. Single-inductor multi-port converters (SIMPCs) enhance power transfer and feature regenerative braking, boosting overall efficiency. This paper takes a closer look at a non-isolated multiport converter that uses smart control strategies to ensure reliable and efficient power for EV applications.

II. LITERATURE SURVEY

[1] **S. R. Khasim and C. Dhanamjayulu** argue that hybrid electric vehicles (HEVs) could be the best alternative to internal combustion engines (ICEs). They emphasize several advantages, like lower emissions, quiet operation, and cost-effectiveness in maintenance and fuel. In their paper, they offer a thorough review of current electric vehicle (EV) architectures. They make numerous comparisons based on key parameters, driving cycles, and the types of electric motors that are commonly employed in EVs. The paper also presents a variety of combinations of hybrid energy storage systems (HESS) used in EV designs, discussing their pros and cons.

[2] **S. Padmanaban, C.Dhanamjayulu, D. Prasad**This hybrid Cascaded H-Bridge MLI generates 9 or 17 voltage levels with fewer switches, reducing cost, size, and improving efficiency. It outperforms similar MLIs in

cost per level, harmonic content, and stability, making it ideal for FACTS and renewable grids.

[3] **Suresh** This four-port buck-boost converter really gets the most out of energy use in electric vehicles. It can switch it up between buck, boost, and buck-boost outputs without needing a transformer. Plus, it supports power flowing both ways and does it with fewer parts, making it super efficient in managing multiple energy sources.

[4] **M. Dhananjaya, D. Ponuru, T. S. Babu.** This paper represents how a SIMO converter is designed. We've broken down how it works and gone over the different modes so that's straightforward and easy to understand. The setup we're suggesting is pretty simple, and we haven't made any assumptions about how the inductor charges or the duty cycle while it operates. It can deliver buck, boost, and buck-boost output voltages, all with independent regulation. One of the major advantages of this design is that it avoids cross regulation problems. This means that sudden changes in inductor and load currents won't disrupt the output voltages. Plus, both our simulations and real-world tests demonstrate just how effectively this converter works.

SOLAR POWER GENERATION

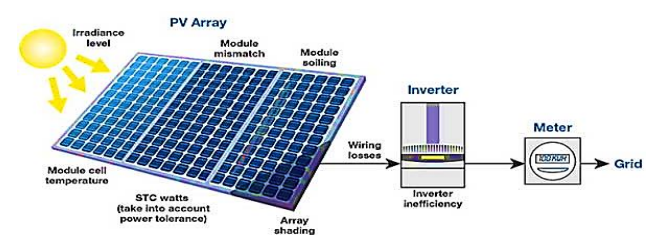


Fig1. solar PV generation

Solar power generation takes sunlight and turns it into electricity using solar photovoltaic (PV) technology. A typical solar PV setup consists of inverters, a mounting system and solar panels. Solar panels catch sunlight and convert it into DC electricity. Then, an inverter changes that DC into AC electricity for homes, businesses, or even back to the power grid. The mounting system holds the panels at just the right angle to soak up the most sunlight.

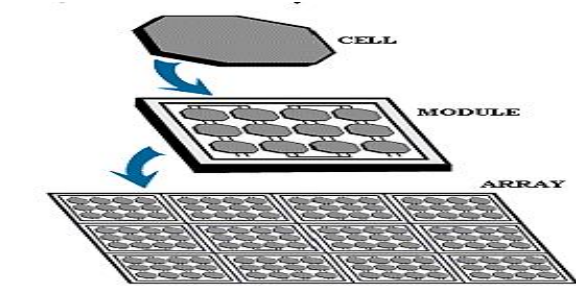


Fig2. Cell Module and Array

A solar cell, often called a PV cell, is a nifty little device that turns sunlight into electricity through something called the photovoltaic effect. Usually made from silicon, these cells are pretty cool because they release electrons when the sun shines on them, which helps create an electric current. PV modules bring together several cells and wrap them in protective glass, while PV arrays take it a step further by combining those modules to crank up the power output. These systems store energy as DC electricity, which can either be used right away or turned into AC power. Depending on the type, their efficiency can range anywhere from 15% to 25%. Plus, with smart techniques like Incremental Conductance, we can tweak their performance to get the most out of them. Various modeling methods help ensure everything runs smoothly, making PV technology a critical player in renewable energy for both homes and utilities.

WORKING OF PV CELL

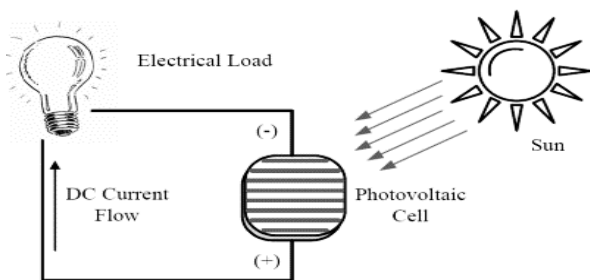


Fig3. working of PV Cell

PV cells convert sunlight into electricity via the photovoltaic effect. A p-n junction guides electrons, generating DC, which can be used, stored, or converted to AC via an inverter. Efficiency depends on semiconductor type, light intensity, and temperature. Advances like multi-junction and perovskite cells improve energy output.

MODELING OF PV CELL

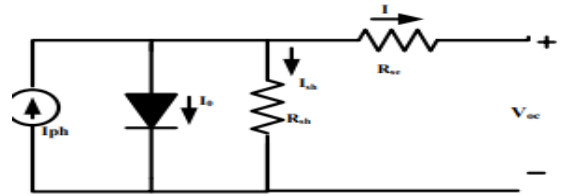


Fig4. Solar cell equivalent model

To understand how a photovoltaic (PV) cell works, it helps to think of its equivalent circuit. This includes a current source, a diode, a series resistance (R_s), and shunt resistance (R_{sh}). We use the Shockley diode equation to figure out the output current (I), factoring in things like the ideality factor (n), thermal voltage (V_t), light-generated current (I_{ph}), and the diode saturation current (I_0). To make our models more accurate, we consider recombination losses using single-diode and double-diode models. Keep in mind that various factors like temperature, light intensity, and material properties can influence performance. So, PV modeling helps us predict voltage-current (V - I) characteristics, overall efficiency, and how these systems fit into broader renewable energy setups.

BATTERY SYSTEM

Batteries are pretty fascinating, aren't they? They store electrical energy through what's known as electrochemical cells, which include an anode, a cathode, and an electrolyte. This setup allows electrons to move around and create a current. You'll find batteries in so many things, from the tiny gadgets we rely on daily to larger renewable energy systems. Some common types you might be familiar with are lead-acid, NiCd, NiMH, Li-ion, Li-poly, alkaline, zinc-carbon, silver oxide, and zinc-air batteries. One great thing about batteries is their portability—they provide energy whenever we need it. Most can be recharged, which helps reduce waste and can save you some cash, too. Plus, there are eco-friendly ways to dispose of batteries properly, making them a more sustainable option. Their versatility and efficiency are what really make them essential today, powering everything from our everyday electronics to electric vehicles and renewable energy storage solutions.

ELECTRIC VEHICLES

ELECTRIC CAR DIAGRAM

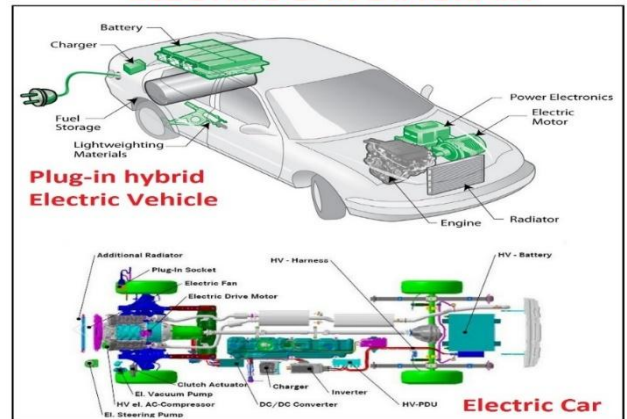


Fig5. Electric Vehicle

Electric vehicles, or EVs, have an interesting history that goes all the way back to 1832! They really started gaining traction in the late 1800s, even before gasoline cars were the main option. Fast forward to today, and EVs are super important for cutting down on carbon emissions, fighting climate change, and reducing our reliance on existing fuels. These cars run on rechargeable batteries and electric motors and even use regenerative braking to boost their efficiency. You'll find a few different types of EVs around, such as hybrid electric vehicles (HEVs), battery electric vehicles (BEVs), plug-in hybrid electric vehicles (PHEVs), and fuel cell electric vehicles (FCEVs). The benefits? We're talking about lower operating costs, zero emissions, and a smoother driving experience. EVs aren't just changing the way we drive; they're also making a big impact in public transportation, businesses, emergency services, and even in industries like agriculture and mining. With technology changing quickly and governments stepping up, EVs are set to play a critical role in a sustainable future.

ELECTRICAL LOAD

Any system or gadget that needs electricity to run, like motors, electronics, lights, or heaters, is considered an electrical load. Three types of loads exist: capacitive (power factor correction units), inductive (motors, transformers), and resistive (lightbulbs, heaters). Depending on demand, they may be variable or fixed. Effective electrical load management is essential for grid stability, system dependability, and energy conservation. Smart grids and load management strategies optimize power distribution in contemporary systems, lowering waste and operating expenses. Designing effective power systems for homes, businesses, and renewable energy applications requires an understanding of electrical loads.

- Balanced and Unbalanced loads
- Linear and nonlinear loads

III. PROPOSED METHOD

MODELING OF PV ARRAY

The PV array model we're proposing relies on a single-diode equivalent circuit. This setup includes a source current, a diode, shunt resistance (Rsh), and series resistance (Rs) to reflect real-world losses. The current generated by the light (Iph) is affected by factors like temperature and sunlight intensity, while the diode equation helps us understand the voltage-current behavior. To get the best performance, MPPT algorithms adjust the operating points automatically, ensuring we're pulling out the maximum power possible. Plus, the model incorporates DC-DC converters and battery storage for effective energy management. This approach improves how we integrate with the grid, enhances system stability, and optimizes solar power use, making it a great fit for

today's renewable energy systems.

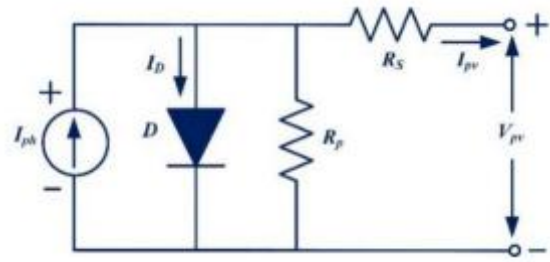


Fig 6. equivalent circuit of a pv cell

In a solar cell, the internal resistances R_s and R_p connect in series and parallel to the diode, as shown in Fig. 6.

$$I_{PV} = \left\{ I_p - I_0 \left[\exp \left(\frac{q(V_{PV} + R_S I_{PV})}{N_S A T K} \right) - 1 \right] - \frac{(V_{PV} + R_S I_{PV})}{N_S R_P} \right\} \quad (1)$$

R_s and R_p are series and parallel resistances, N_s and N_p are PV cell counts, K is Boltzmann's constant (1.3806503102 J/K), T is temperature, A is the ideality factor, and I_{ph} is the photocurrent based on irradiation and temperature.

$$I_p = [I_{SOC-STC} + K_i (T - T_{STC})] - \left(\frac{G}{G_{STC}} \right) \quad (2)$$

$I_{SOC-STC}$ represents this (SCC) under standard conditions (STC), K_i is the coefficient of SCC, G (in W/m²) represents the irradiation of the solar cell receives, G_{STC} (1000W/m²) is the solar flux at STC levels, and T_{STC} (25°C) is the cell's temperature at STC.

$$I_0 = \left\{ \frac{I_{SOC-STC} + K_i (T - T_{STC})}{\exp [(V_{OCV-STC} + K_v (T - T_{STC}) / A V_{th})]} \right\} \quad (3)$$

$V_{OCV-STC}$ represents the no-load voltage at STC, K_v denotes the OCV coefficient, and V_{th} refers to the thermal equivalent voltage of the cell, which can all be found on the module's datasheet.

$$P_{PV} = V_{PV} \times N_p \left(I_{ph} - I_0 \exp \left(\frac{q V_{PV}}{N_S A K T} \right) - \left(\frac{V_{PV}}{N_S} \right) \right) \quad (4)$$

Fig. 7 illustrates the voltage-current characteristics of a PV cell. The graph represents the operating point of a solar PV system is quite unstable, fluctuating between zero and the OCV. The maximum power point tracking is critical—it's the one point that gives us the highest power output based on the solar module's design, factoring in changes in temperature and solar radiation (MPP). VMPP and IMPP indicate the voltage and current at this critical moment, as shown in FIGURE 7.

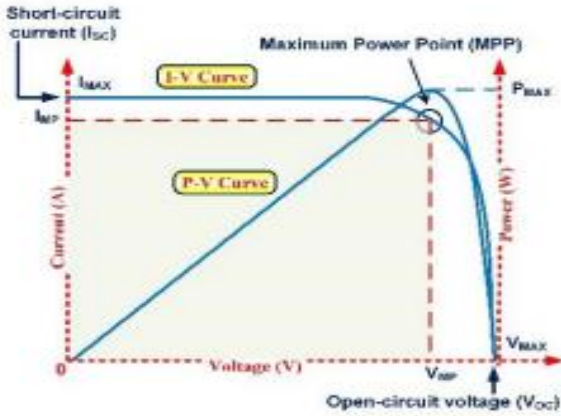


Fig 7. voltage-current characteristics of a solar cell

A. MPPT CONTROLLER

MPPT, or Maximum Power Point Tracking, helps solar panels get the most power by adjusting to changes in the weather. There are several ways to do this: some use AI, while others use more straightforward methods like the Hill Climb (HC) or Perturb and Observe (P&O) techniques. P&O and HC are easy to understand, but they don't perform as well in consistent conditions. On the other hand, Incremental Conductance (INC) reduces oscillations and provides smoother performance. While AI can boost efficiency, it does require more resources. Indirect methods estimate the maximum power point by looking at voltage and current characteristics.

TABLE 1. Parameters of 215W solar panel.

Open circuit voltage (V_{oc})	36.3V
The voltage at maximum power point (V_{MPP})	34V
The voltage at maximum power point (V_{MPP})	35V
Short circuit current (I_{sc})	7.84A
Maximum power	213.15W
Diode saturation current (I_0)	$2.9259 \times 10^{-10}A$
Current at maximum power point (I_{MPP})	7.35A
Diode ideality factor	0.98117

B. MPPT WITH ARTIFICIAL NEURAL NETWORK

This para discusses how we can use an Artificial Neural Network (ANN) to find the MPP in solar systems. To do this, we set up a three-layer ANN, which you can see in FIGURE 8. The ANN takes temperature (T) and irradiance (G) as inputs and gives us the MPP voltage (V_{mpp}) as an output. To train the ANN effectively, we need to gather some data for both the input and output variables. This allows us to calculate the weights of the neurons at different levels. You can collect solar PV data and program it in MATLAB. There are various methods to train the ANN, but in this article, we use the backpropagation approach to minimize training errors.

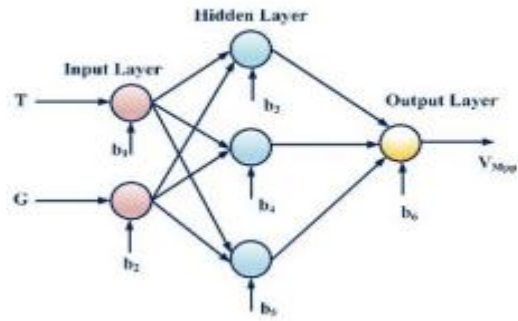


Fig 8. neural network structure.

After training the artificial neural network (ANN), we tweak the neuron weights to get V_{mpp} as the output for specific temperature (T) and solar flux(G) values. By looking at the voltage-current (V-I) characteristics, we can determine I_{mpp} and then calculate the maximum power (Pmax) by multiplying V_{mpp} and I_{mpp} together. The photovoltaic (PV) system, which has an MPPT tracker (see Figure 8), includes a converter and a control unit that uses an ANN to manage the chopper's duty cycle in real-time.

$$D = 1 - \sqrt{\frac{V_{mpp}}{I_{mpp}} \times \frac{I_0}{V_0}} \tag{5}$$

IMPLEMENTED DC-DC CONVERTER

This new multi-port DC-DC converter is designed to work smoothly with both solar panels (V_{pv}) and battery sources (V_{bat}), using just one inductor, four switches, four diodes, and two capacitors. Since electric vehicles (EVs) often need power from various sources, this setup makes sure that everything runs efficiently. Load resistances (R_1 , R_2) help us figure out how well the power is distributed, while the converter skillfully boosts and fine-tunes output voltages for multilevel inverters. It's flexible enough to handle different voltage needs, and the four switches are key for smart power management, making it a dependable choice for EV applications. Check out FIGURE 9 to see how the energy flows and how the components work together.

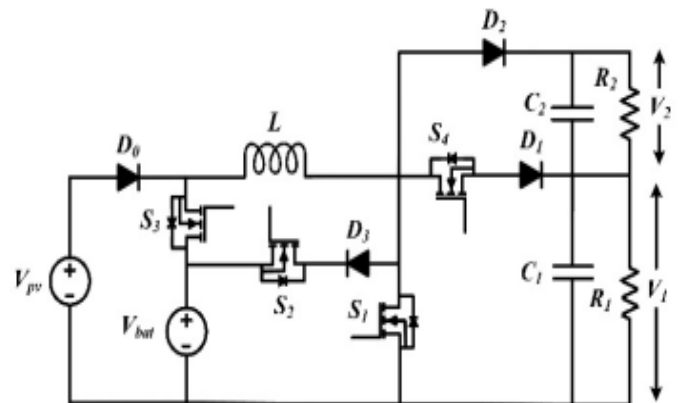


Fig 9. Implemented poly port converter with two inputs and outputs

The converter is set up to let the solar PV (V_{pv}) charge the battery (V_{bat}), but it doesn't work in reverse. So, the PV acts as the main power source, while the battery just stores energy. It has two modes: one for when the battery is supplying power—like during peak demand—and another for when it's charging—typically when demand is lower. In discharging mode, switches S_1 , S_3 , and S_4 are turned on to power the load, while S_2 is off. In charging mode, V_{pv} supplies power to both the load and charges V_{bat} , with S_1 , S_2 , and S_4 on, and S_3 off. The converter really does a good job at balancing input power with the load, helping to keep ripple current down. Most of the time, it runs in continuous conduction mode (CCM), but it switches to discontinuous conduction mode (DCM) when the power levels drop. For more details on these modes and how they are evaluated, check out Section IV.

BATTERY DISCHARGING MODE:

When the battery is discharging, power is sourced from V_{pv} and V_{bat} , with switches S_1 , S_3 , and S_4 active while S_2 is turned off. S_1 controls the inductor current, S_3 keeps the total output voltage (V_T) steady, and S_4 manages V_{pv} . There are four main switching scenarios:

SWITCHING CONDITION 1 ($0 < t < D_3T$): both S_1 and S_3 are on, allowing V_{bat} to charge the inductor L , while the capacitors discharge to the load and the equations regarding this switching condition is shown below. And it is represented by the diagram 10(a).

$$\begin{aligned} L \frac{di_L}{dt} &= V_{pv} \\ C_1 \frac{dV_1}{dt} &= -\frac{V_1}{R_1} \\ C_2 \frac{dV_2}{dt} &= -\frac{V_2}{R_2} \end{aligned} \tag{6}$$

SWITCHING CONDITION 2 ($D_3T < t < D_1T$): S_1 is on and S_3 is off, so V_{pv} charges L while the capacitors supply power to the load. You'll find the relevant equations for the capacitors and inductors in equation (7). One can find their equations applicable to this operation detailed in equation (7).

$$\begin{aligned} L \frac{di_L}{dt} &= V_{pv} \\ C_1 \frac{dV_1}{dt} &= -\frac{V_1}{R_1} \\ C_2 \frac{dV_2}{dt} &= -\frac{V_2}{R_2} \end{aligned} \tag{7}$$

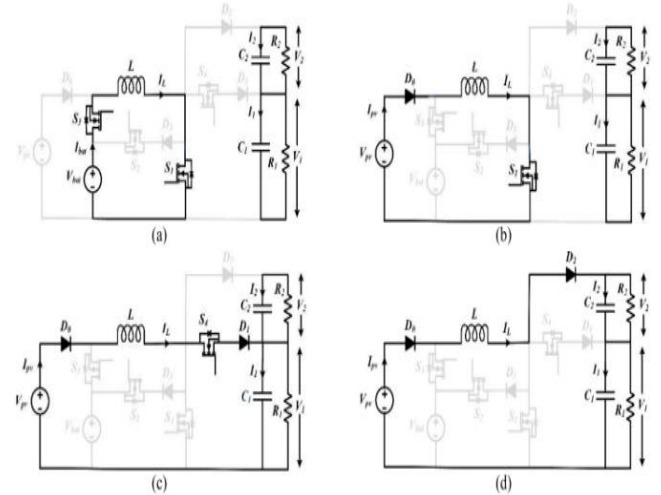


Fig 10. Discharging modes of battery: (a) Mode-1 (b) Mode-2 (c) Mode-3 (d) Mode-4.

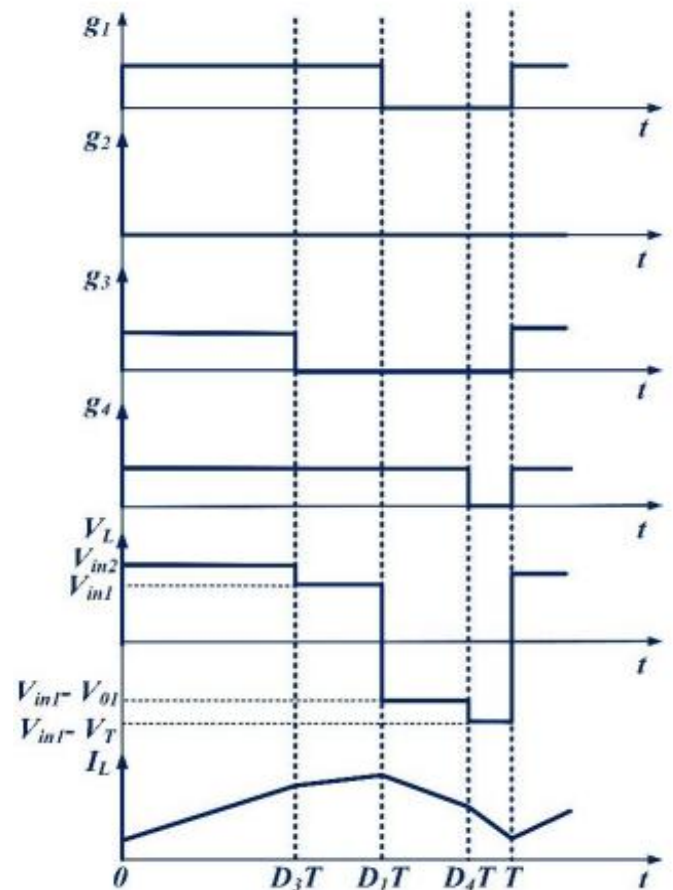


Fig 11. Typical steady-state waveform while discharging a battery.

SWITCHING CONDITION 3 ($D_1T < t < D_4T$): with S_1 and S_3 off and S_4 on, the inductor provides power to the load, charging C_1 and discharging C_2 . You can find their equations applicable to this operation detailed in equation (8). The corresponding circuit model of the

converter is illustrated in FIGURE 10(c)

$$\begin{aligned} L \frac{di_L}{dt} &= V_{pv} - V_1 \\ C_1 \frac{dV_1}{dt} &= i_L - \frac{V_1}{R_1} \\ C_2 \frac{dV_2}{dt} &= -\frac{V_2}{R_2} \end{aligned} \quad (8)$$

SWITCHING CONDITION 4 (D4T < t < T): when all switches are off, the energy from the inductor charges both C1 and C2 and powers the load. The capacitors are getting charged now. The corresponding circuit model of the converter is illustrated in FIGURE 10(d), and You can find their equations applicable to this operation detailed in equation (9).

$$\begin{aligned} L \frac{di_L}{dt} &= V_{pv} - (V_1 + V_2) \\ C_1 \frac{dV_1}{dt} &= i_L - \frac{V_1}{R_1} \\ C_2 \frac{dV_2}{dt} &= i_L - \frac{V_2}{R_2} \end{aligned} \quad (9)$$

BATTERY CHARGING MODE:

When the battery is charging, the V_{pv} sends power to both V_{bat} and the load whenever there's extra energy around. Switches S1, S2, and S4 are turned on, while S3 stays off. S1 is in charge of V_T, S2 takes care of I_{bat}, and S4 tweaks V_{pv}. There are four situations to consider:

SWITCHING CONDITION 1 (0 < t < D1T): With S1 on, V_{pv} charges the inductor L while C1 and C2 supply power to the load. You can find their equations applicable to this operation detailed in equation (10). Check out FIGURE 13(a) for a visual of the circuit in this mode.

$$\begin{aligned} L \frac{di_L}{dt} &= V_{pv} \\ C_1 \frac{dV_1}{dt} &= -\frac{V_1}{R_1} \\ C_2 \frac{dV_2}{dt} &= -\frac{V_2}{R_2} \end{aligned} \quad (10)$$

SWITCHING CONDITION 2 (D1T < t < D2T): When S1 is off and S2 is on, the inductor discharges to charge V_{bat}, and the capacitors keep the energy flowing to the load. You can find their equations applicable to this operation detailed in equation (11). Check out FIGURE 13(b) for a visual of the circuit in this mode.

$$\begin{aligned} L \frac{di_L}{dt} &= V_{pv} - V_{bat} \\ C_1 \frac{dV_1}{dt} &= -\frac{V_1}{R_1} \\ C_2 \frac{dV_2}{dt} &= -\frac{V_2}{R_2} \end{aligned} \quad (11)$$

SWITCHING CONDITION 3 (D2T < t < D4T): If both S1 and S2 are off and S4 is active, the inductor discharges to C1 and R1 while C2 powers R2. One can find their equations applicable to this operation detailed in equation (12). Check out FIGURE 13(c) for a visual of the circuit in this mode.

$$\begin{aligned} L \frac{di_L}{dt} &= V_{pv} - V_1 \\ C_1 \frac{dV_1}{dt} &= i_L - \frac{V_1}{R_1} \\ C_2 \frac{dV_2}{dt} &= -\frac{V_2}{R_2} \end{aligned} \quad (12)$$

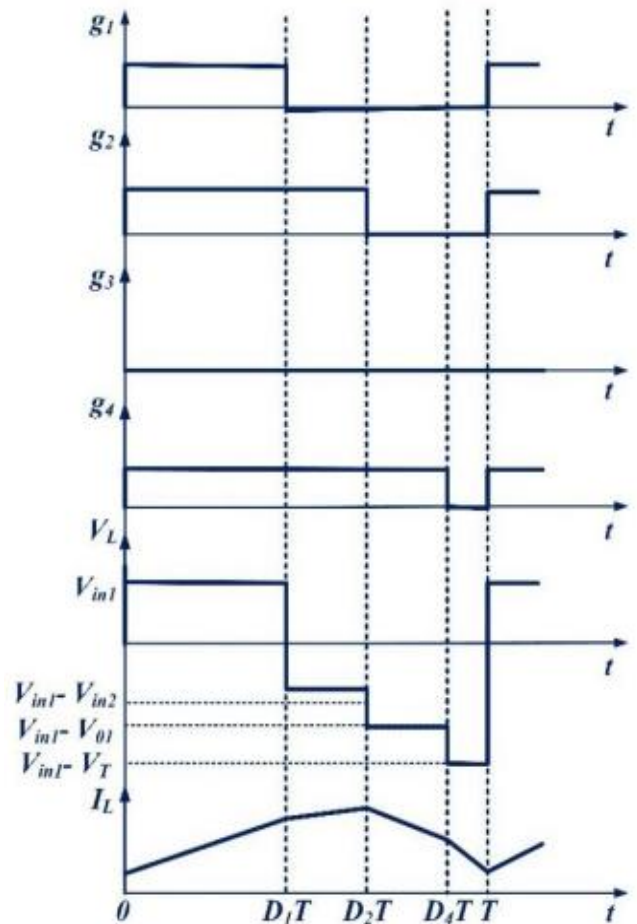


Fig 12. The typical steady-state waveform in the charging mode of a battery

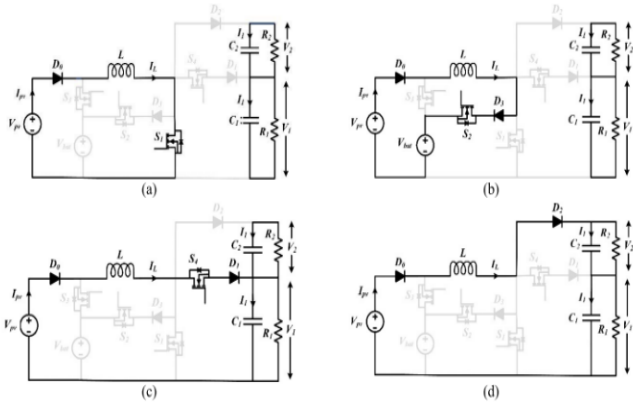


Fig 13. charging modes of a battery: (a) Mode-1 (b) Mode-2 (c) Mode-3 (d) Mode-4.

SWITCHING CONDITION 4 (D4T < t < T): Lastly, if everything is off, energy from the inductor fills up C1 and C2, which then power the load. One can find their equations applicable to this operation detailed in equation (13). Check out FIGURE 13(d) for a visual of the circuit in this mode.

$$\begin{aligned}
 L \frac{di_L}{dt} &= V_{pv} - (V_1 + V_2) \\
 C_1 \frac{dV_1}{dt} &= i_L - \frac{V_1}{R_1} \\
 C_2 \frac{dV_2}{dt} &= i_L - \frac{V_2}{R_2}
 \end{aligned} \tag{13}$$

DESIGNING OF THE PROPOSED CONVERTER:

ENERGETIC MODELLING: You can control the converter with switches S1, S2, S3, and S4 by tweaking their duty cycles to manage output voltages and keep the battery charging or discharging properly. To make everything work smoothly, we need to set up a closed-loop controller based on energetic models for two different operations: one for when the battery is discharging (where Vpv and Vbat supply power to the load) and another for when it's charging (during which Vpv powers the load and charges Vbat). Each of these operations needs its own specialized controller to really shine.

Discharging condition of a battery:

When we kicked off our controller design project, we started with a small-signal model. This is an important step for handling closed-loop control in multi-port converters, which can be a bit more detailed than your typical systems. Figuring out the transfer functions can be tricky, so we rely on matrix representations and software to help us create Bode plots. Our model considers both the DC levels and slight adjustments in duty ratios, state variables, and input excitations. We keep a close eye on how the converter performs by tracking the inductor current, $i_L(t)$, and the voltages across the capacitors, $V_1(t)$ and $V_2(t)$.

From that, we can build our small-signal equations

$$\begin{aligned}
 i_L(t) &= I_L + \hat{I}_L(t) \\
 V_1(t) &= V_1 + \hat{V}_1(t) \\
 V_2(t) &= V_2 + \hat{V}_2(t)
 \end{aligned}$$

accordingly.

$$\begin{aligned}
 d_1(t) &= D_1 + \hat{d}_1(t) \\
 d_2(t) &= D_2 + \hat{d}_2(t) \\
 d_3(t) &= D_3 + \hat{d}_3(t) \\
 d_4(t) &= D_4 + \hat{d}_4(t)
 \end{aligned} \tag{14}$$

$$\begin{aligned}
 L \frac{d\hat{I}_L(t)}{dt} &= (V_{bat} - V_{pv})\hat{d}_3(t) \\
 &+ \hat{D}_3 V_{bat}(t) + (1 - D_3)V_{pv}(t) \\
 &- (1 - D_1)\hat{V}_1(t) \\
 &+ (D_4 - 1)\hat{V}_2(t) + V_1\hat{d}_1(t) + V_2\hat{d}_4(t) \\
 C_1 \frac{d\hat{V}_1(t)}{dt} &= -I_L\hat{d}_1(t) + (1 - D_1)\hat{I}_L(t) - \frac{\hat{V}_1(t)}{R_1} \\
 C_2 \frac{d\hat{V}_2(t)}{dt} &= -I_L\hat{d}_4(t) + (1 - D_4)\hat{I}_L(t) - \frac{\hat{V}_2(t)}{R_2}
 \end{aligned} \tag{15}$$

The system uses a state-space model to display its dynamics. It includes state variables like $i_L(t)$, $V_{bat}(t)$, and $V_{pv}(t)$, which together form a matrix representation of the converter's behavior.

$$\begin{aligned}
 \frac{dX}{dt} &= AX + BU \\
 Y &= CX + DU
 \end{aligned} \tag{16}$$

the matrices for X, Y, and U appear as follows:

$$X = \begin{bmatrix} \hat{I}_L(t) \\ \hat{V}_1(t) \\ \hat{V}_2(t) \end{bmatrix}, Y = \begin{bmatrix} \hat{V}_T(t) \\ \hat{I}_b(t) \end{bmatrix}, U = \begin{bmatrix} \hat{d}_4(t) \\ \hat{d}_3(t) \\ \hat{d}_1(t) \end{bmatrix}. \tag{17}$$

By comparing equation 15 and 16. We get,

$$\begin{aligned}
 A &= \begin{bmatrix} 0 & \frac{(D_1-1)}{L} & \frac{(D_4-1)}{L} \\ \frac{(1-D_1)}{C_1} & -\frac{1}{R_1 C_1} & 0 \\ \frac{(1-D_4)}{C_2} & 0 & -\frac{1}{R_2 C_2} \end{bmatrix} \\
 B &= \begin{bmatrix} \frac{V_2}{L} & \frac{V_1}{L} & \frac{(V_{bat}-V_{pv})}{L} \\ 0 & -\frac{I_L}{C_1} & 0 \\ -\frac{I_L}{C_1} & 0 & 0 \end{bmatrix} \\
 C &= \begin{bmatrix} 0 & 1 & 0 \\ 0 & 1 & 1 \\ D_3 & 0 & 0 \end{bmatrix}, D = \begin{bmatrix} 0 & 0 & 0 \\ 0 & 0 & 0 \\ 0 & I_L & 0 \end{bmatrix}
 \end{aligned} \tag{18}$$

Where V_{pv} and V_{bat} are the input voltages. V_1 and V_2 are also the output voltages. Other than the duty cycles for switches D_1 , D_3 , and D_4 , and I_L , we know all the parameters in the A, B, C, and D matrices. To calculate

the inductor current.

$$I_L = \frac{I_b}{D_3} \tag{19}$$

Here, I_b is the battery current and D_1 , D_3 , and D_4 are the only unknowns in the stated matrices. The steady-state equations help us determine the duty cycles for the switches, represented as follows:

$$\begin{bmatrix} V_1 & V_{bat} - V_{pv} & V_2 \\ R_1 I_b & V_1 & 0 \\ 0 & V_2 & R_2 I_b \end{bmatrix} \begin{bmatrix} D_1 \\ D_3 \\ D_4 \end{bmatrix} = \begin{bmatrix} V_1 + V_2 - V_{pv} \\ R_1 I_b \\ R_2 I_b \end{bmatrix} \tag{20}$$

The duty cycles are derived from the matrix equation and summarized in matrices A, B, C, and D. The small-signal model defines the control variables $d_1(t)$, $d_3(t)$, and $d_4(t)$ as state variables, leading to the converter's transfer function matrix.

$$G = C(SI - A)^{-1}B + D \tag{21}$$

Where

$$y = Gu \tag{22}$$

The transfer function matrix GG has a rank of 3, matching the three control variables per equation (17).

$$\begin{bmatrix} y_1 \\ y_2 \\ y_3 \end{bmatrix} = \begin{bmatrix} g_{11} & g_{12} & g_{13} \\ g_{21} & g_{22} & g_{23} \\ g_{31} & g_{32} & g_{33} \end{bmatrix} \begin{bmatrix} u_1 \\ u_2 \\ u_3 \end{bmatrix} \tag{23}$$

Each g_{ij} represents the transfer function from input u_j to output y_i , resulting in three distinct transfer functions.

$$\begin{aligned} \frac{\hat{V}_1(s)}{d_4(s)} &= g_{11} \\ \frac{\hat{V}_T(s)}{d_3(s)} &= g_{22} \\ \frac{\hat{I}_b(s)}{d_1(s)} &= g_{23} \end{aligned} \tag{24}$$

Charging condition of a battery:

When in charge mode (S_1, S_2, S_4 on, S_3 off), (V_{pv}) charges the battery and loads. Simplified small-signal equations can be obtained by linearizing equation (14) and substituting it into (10)–(13).

$$\begin{aligned} L \frac{d\hat{I}_L(t)}{dt} &= \hat{V}_{pv}(t) + V_{bat}\hat{d}_1(t) \\ &\quad + (D_1 - D_2)\hat{V}_{bat}(t) + (V_1 - V_{bat})\hat{d}_2(t) \\ &\quad + V_2\hat{d}_4(t) + (D_2 - 1)\hat{V}_1(t) - (1 - D_4)\hat{V}_2(t) \\ C_1 \frac{d\hat{V}_1(t)}{dt} &= -I_L\hat{d}_2(t) + (1 - D_1)\hat{I}_L(t) - \frac{\hat{V}_1(t)}{R_1} \\ C_2 \frac{d\hat{V}_2(t)}{dt} &= -I_L\hat{d}_4(t) + (1 - D_4)\hat{I}_L(t) - \frac{\hat{V}_2(t)}{R_2} \end{aligned} \tag{25}$$

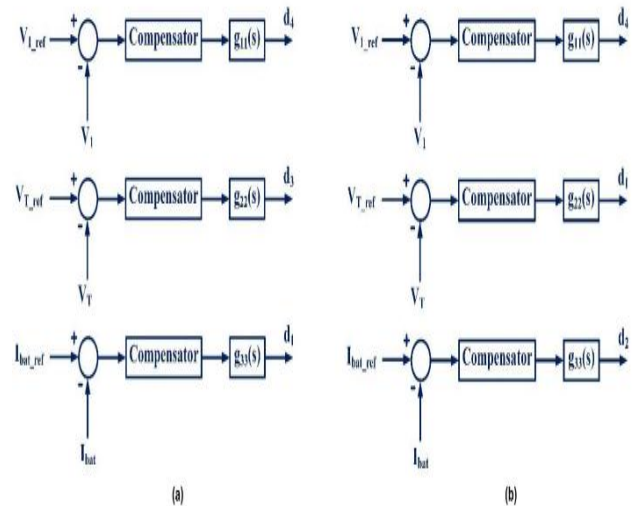


Fig 14. The control framework of the created converter (a) Discharging phase (b) Charging phase

These formulas can be represented using state-space equations. In this operational mode, which resembles the battery discharging phase, the state variables comprise $i_L(t)$, $V_1(t)$, and $V_2(t)$. Below are some examples of these state variables along with the input and output matrices:

$$X = \begin{bmatrix} \hat{I}_L(t) \\ \hat{V}_1(t) \\ \hat{V}_2(t) \end{bmatrix}, y = \begin{bmatrix} \hat{V}_1(t) \\ \hat{V}_T(t) \\ \hat{I}_b(t) \end{bmatrix}, u = \begin{bmatrix} \hat{d}_4(t) \\ \hat{d}_1(t) \\ \hat{d}_2(t) \end{bmatrix}. \tag{26}$$

In this context, $V_T(t)$ is equal to the $V_1(t)$ plus $V_2(t)$. the matrices are shown below.

$$\begin{aligned}
 A &= \begin{bmatrix} 0 & \frac{(D_2-1)}{L} & \frac{(D_4-1)}{L} \\ \frac{(1-D_2)}{C_1} & -\frac{1}{R_1 C_1} & 0 \\ \frac{(1-D_4)}{C_2} & 0 & -\frac{1}{R_2 C_2} \end{bmatrix} \\
 B &= \begin{bmatrix} \frac{V_{bat}}{L} & \frac{(V_1-V_{bat})}{L} & \frac{V_2}{L} \\ 0 & -\frac{I_L}{C_1} & 0 \\ 0 & 0 & -\frac{I_L}{C_1} \end{bmatrix} \\
 C &= \begin{bmatrix} 0 & 1 & 0 \\ 0 & 1 & 1 \\ D_2 - D_1 & 0 & 0 \end{bmatrix}, D = \begin{bmatrix} 0 & 0 & 0 \\ 0 & 0 & 0 \\ -I_L & I_L & 0 \end{bmatrix}
 \end{aligned} \tag{27}$$

The I_L can be described with the following equation:

$$I_L = \frac{I_b}{D_2 - D_1} \tag{28}$$

Here I_b represents the target battery current value. And the duty cycles for D_1 , D_2 , and D_4 are the unknowns' values determined using steady-state equations.

$$\begin{bmatrix} V_{bat} & V_1 - V_{bat} & V_2 \\ -V_1 & V_1 + R_1 I_b & 0 \\ -V_2 & V_2 & R_2 I_b \end{bmatrix} \begin{bmatrix} D_1 \\ D_2 \\ D_4 \end{bmatrix} = \begin{bmatrix} V_1 + V_2 - V_{pv} \\ R_1 I_b \\ R_2 I_b \end{bmatrix} \tag{29}$$

The below TF matrix represent the small signal converter model

$$G = C(SI - A)^{-1} B + D \tag{30}$$

Where,

$$y = Gu \tag{31}$$

here y and u are the output and input vectors of the system, respectively.

$$\begin{aligned}
 \frac{\hat{V}_1(s)}{d_4(s)} &= g_{11} \\
 \frac{\hat{V}_T(s)}{d_1(s)} &= g_{22} \\
 \frac{\hat{I}_b(s)}{d_2(s)} &= g_{33}
 \end{aligned} \tag{32}$$

when charging the battery, if the battery current and load power are low, the converter might switch to discontinuous conduction mode (DCM). For converters in DCM, the I_L needs to stay below the current ripple.th

$$\begin{aligned}
 V_{bat} D_1 + (V_1 - V_{bat}) D_2 + V_2 D_4 &= V_1 + V_2 - V_{pv} \\
 -I_L D_2 + I_L &= \frac{V_1}{R_1} \\
 -I_L D_4 + I_L &= \frac{V_2}{R_2}
 \end{aligned} \tag{33}$$

The below equation represents the ripple in the inductor current under charging condition.

$$\Delta I_L = \frac{V_{pv} D_1 T_s}{L} \tag{34}$$

As a result, if the conditions met in equations (28), (33), and (34) hold true, the converter will operate in DCM.

$$\begin{aligned}
 I_L &= \frac{V_2}{R_1(1 - D_1)} < \frac{V_{pv} D_1 T_s}{L} \\
 I_L &= \frac{V_2}{R_2(1 - D_4)} < \frac{V_{pv} D_1 T_s}{L} \\
 I_L &= \frac{I_b}{(D_2 - D_1)} < \frac{V_{pv} D_1 T_s}{L}
 \end{aligned} \tag{35}$$

$$\begin{aligned}
 R_1 &> \frac{V_1 L f_s}{D_1(1 - D_2) V_{pv}} \\
 R_2 &> \frac{V_2 L f_s}{D_1(1 - D_4) V_{pv}} \\
 I_b &> \frac{D_1(D_2 - D_1) V_{pv}}{L f_s}
 \end{aligned} \tag{36}$$

CONTROLLER DESIGN: In the sections above, we discussed the two operating modes and their TF. Because each mode has its own unique transfer function, we need to create a separate controller for each one. You can find diagrams of the control blocks for both operation modes in FIGURE 14. For battery discharging mode, both R_1 and R_2 are set to 35Ω , while during battery charging, they're set to 70Ω . The values can be seen rewritten in equations (37) and (38) below.

$$g_{11} = \frac{\hat{V}_1(s)}{\hat{d}_4(s)} = \frac{\left(\frac{V_2(1-D_1)}{L C_1}\right) S + \left(\frac{V_2(1-D_1)}{R_2 C_1 C_2} - \frac{I_L(1-D_1)(D_1-1)}{L C_1 C_2}\right)}{S^3 + \left(\frac{R_1 C_1 + R_2 C_2}{R_1 R_2 C_1 C_2}\right) S^2 + \left(\frac{L + (1-D_1)^2 R_1 R_2 C_2 + (D_1-1)^2 R_1 R_2 C_1}{L R_1 R_2 C_1 C_2}\right) S + \left(\frac{R_1(1-D_1)^2 + (D_1-1)^2 R_2}{L R_1 R_2 C_1 C_2}\right)} \tag{37}$$

$$g_{22} = \frac{\hat{V}_T(s)}{\hat{d}_3(s)} = \frac{\left(\frac{V_{bat}-V_{pv}}{L}\right) \left(\frac{1-D_1}{C_1} - \frac{D_1-1}{C_2}\right) S + \left(\frac{1-D_1}{R_2 C_1 C_2} - \frac{D_1-1}{R_1 C_1 C_2}\right) \left(\frac{V_{bat}-V_{pv}}{L}\right)}{S^3 + \left(\frac{R_1 C_1 + R_2 C_2}{R_1 R_2 C_1 C_2}\right) S^2 + \left(\frac{L + (1-D_1)^2 R_1 R_2 C_2 + (D_1-1)^2 R_1 R_2 C_1}{L R_1 R_2 C_1 C_2}\right) S + \left(\frac{R_1(1-D_1)^2 + (D_1-1)^2 R_2}{L R_1 R_2 C_1 C_2}\right)} \tag{38}$$

CONTROLLER FOR BATTERY DISCHARGING MODE: So, when we talk about battery discharging mode, we're actually looking at three transfer functions in the frequency domain using some software. The Bode plot for g_{11} isn't looking great. it shows that the phase margin isn't enough, which means the system isn't really stable. To fix that, we're throwing in a lead compensator to step up the stability.

$$K(s) = K \frac{S + Z}{S + P} \tag{39}$$

TABLE 2. Parameters of the converter

Parameters	Ratings
Inductor, L	2.5mH
Capacitor, C ₁	1000µF
Capacitor, C ₂	1000µF
Solar PV voltage, V _{pv}	35V
Battery voltage, V _{batt}	48V
Switching frequency, F _s	10kHz
dSPACE controller	RT11104

A lead compensator improves stability for g₁₁, as shown in FIGURE 15(b). Similarly, g₂₂ lacks phase margin, requiring another lead compensator, based on its transfer function.

$$K_{lead}(s) = 2.8960 \frac{S + 2098.9}{S + 16982} \quad (40)$$

Alright, so a lead compensator kind of steps in and lowers the DC gain, which, unfortunately, cranks up the steady-state error a bit. To sort that out, we just add a lag compensator, making sure its zero is set to be ten times lower than the crossover frequency.

$$K_{lag}(s) = K \frac{S + Z}{S + P} \quad (41)$$

So, with K set to 1K, P at 58.345, and Z at 583.45, the lead-lag compensators are really doing their thing to make everything feel more stable, just like you can see in FIGURE 16(b). The switch S1 is helping to keep the inductor current in check, which ensures the battery current stays within safe limits, just like we talked about in equation (42).

$$g_{33} = \frac{\hat{i}_b(s)}{\hat{d}_1(s)} = \frac{\left(\frac{V_1 D_1}{L}\right) S^2 + \left[\frac{D_1 V_1}{R_1 C_1} + \frac{1}{R_2 C_2}\right] S + \left(\frac{D_1 V_1}{L R_1 R_2 C_1 C_2} + \frac{I_1 (1-D_1) D_1}{L R_2 C_1 C_2}\right)}{S^3 + \left(\frac{R_1 C_1 + R_2 C_2}{R_1 R_2 C_1 C_2}\right) S^2 + \left(\frac{L + (1-D_1)^2 R_1 R_2 C_2 + (D_1 - 1)^2 R_1 R_2 C_1}{L R_1 R_2 C_1 C_2}\right) S + \left(\frac{R_1 (1-D_1)^2 + (D_1 - 1)^2 R_2}{L R_1 R_2 C_1 C_2}\right)} \quad (42)$$

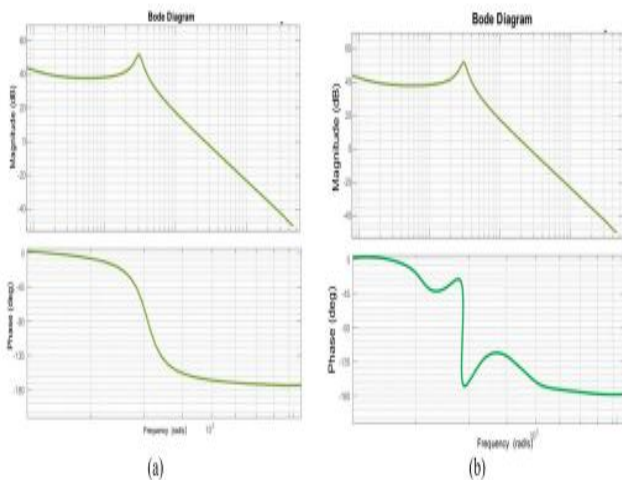


FIGURE 15. Here are the bode plots for g₁₁(s): (a) before we added compensation and (b) after we applied the compensator.

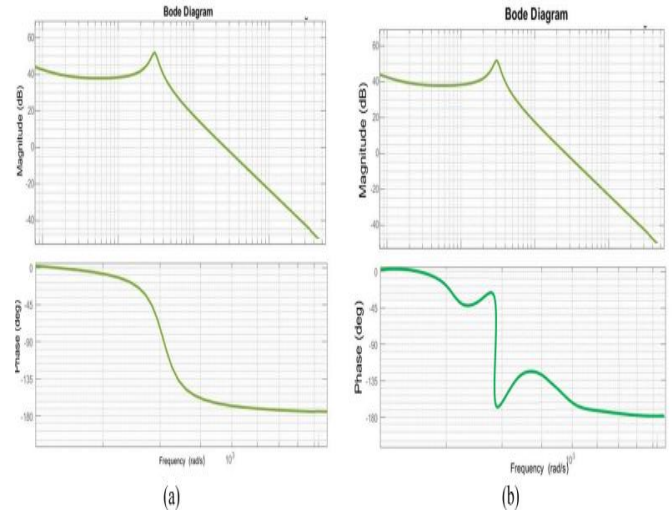


Fig 16. Here are the bode plots for g₂₂(s): (a) before we added compensation and (b) after we applied the compensate

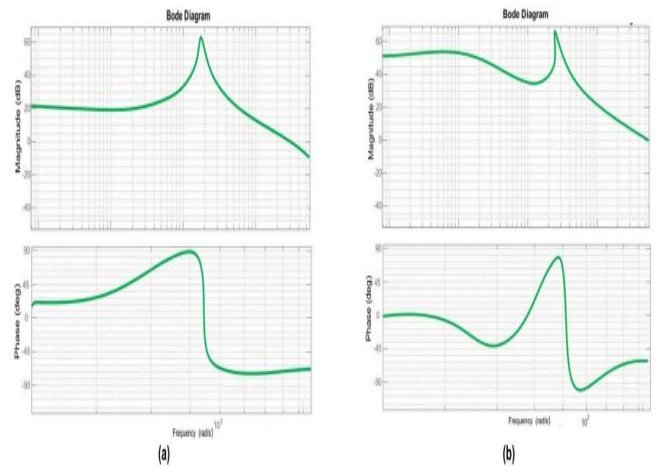


Fig 17. Here are the bode plots for g₃₃(s): (a) before we added compensation and (b) after we applied the compensator.

FIGURE 17(a) shows g₃₃ is stable but has low DC gain. A lag compensator improves precision, with results shown in FIGURE 17(b).

$$K_{lag}(s) = \frac{S + 200}{S + 5} \quad (43)$$

Battery Charging Controller Design: In this mode, switches S1, S2, and S4 are activated, while S3 is turned off, just like we discussed earlier. We use switch S4 to control the voltage output, V₁. Check out FIGURE 15(a) for the bode diagram. To deal with a shortage in phase margin, we need a lead compensator. This leads us to the following transfer function for constructing the lead compensator:

$$K_{lead}(s) = 2.9 \frac{S + 482.7}{S + 4065.8} \quad (44)$$

Next, we introduce a lag-type compensator into our system to help reduce steady-state error:

$$K_{lag}(s) = \frac{S + 140}{S + 14} \quad (45)$$

In FIGURE 15(b), you can see the bode plot after we've applied the lead-lag compensator. Switch S1 also plays a role in managing the total output voltage, VT, during this mode of operation. Take a look at FIGURE 16(a) and 16(b) for the g22 bode diagram. Here, the g22 phase margin isn't enough, so we represent the corresponding compensator below

$$K_{lead}(s) = 2.9 \frac{S + 585.4}{S + 4937} \quad (46)$$

We also bring in a lag compensator to cut down on steady-state error:

$$K_{lag}(s) = \frac{S + 170}{S + 17} \quad (47)$$

Again, you can refer to FIGURE 15(b) for the bode diagram after compensation. Besides, switch S2 is used to manage the battery charging current. Take a look at FIGURE 17(a) and 17(b) for the g33 bode diagram. As you can see, the phase margin is now adequate, meaning we don't need further stabilization, as shown in the diagram. Just a lag compensator is enough to lower steady-state inaccuracies.

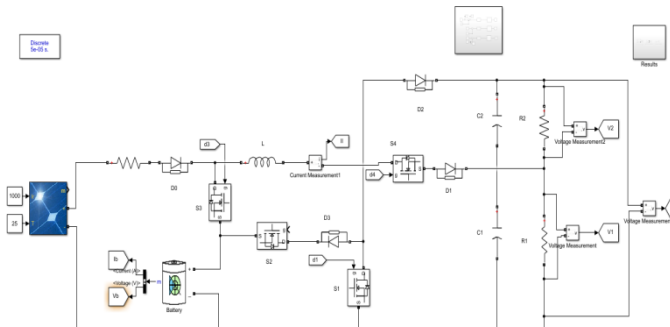
$$K_{lag}(s) = \frac{S + 267.4}{S + 2.67} \quad (48)$$

Finally, FIGURE 20(b) captures the bode diagram post-compensation. You can determine the inductor and capacitor values using the following relationships:

$$L = \frac{(V_{in} + V_b) \times d_2}{2 \times \Delta V_{O1} \times f_s} \quad (49)$$

$$C_1 = C_2 = \frac{V_{O1} \times d_1}{2 \times \Delta V_{O1} \times f_s \times Z_{O1}} \quad (50)$$

V. SIMULATION RESULTS DISCHARGING MODE:



Simulink Model of the System

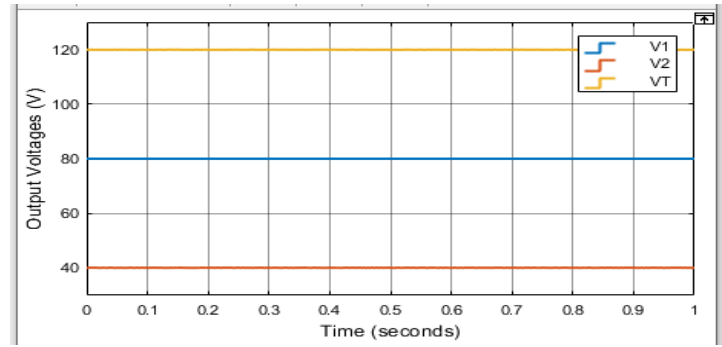
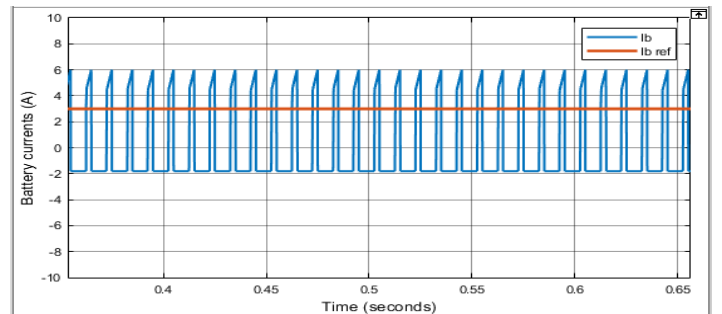
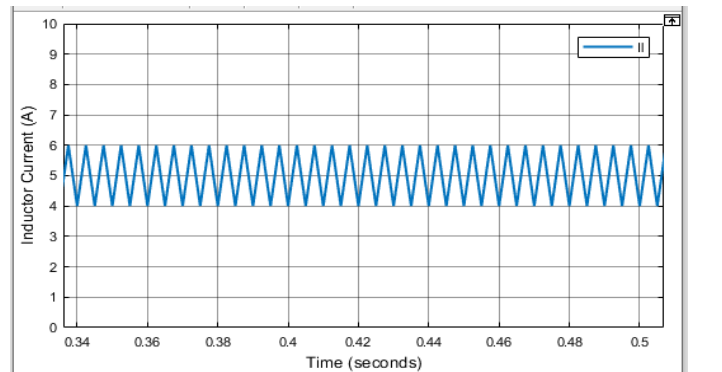


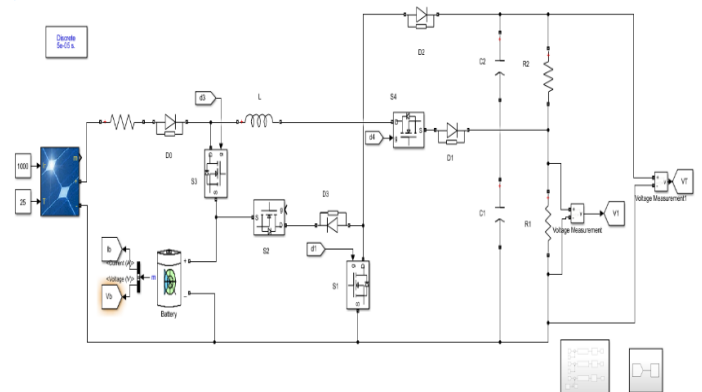
Fig 18. output voltage of a battery during discharging mode



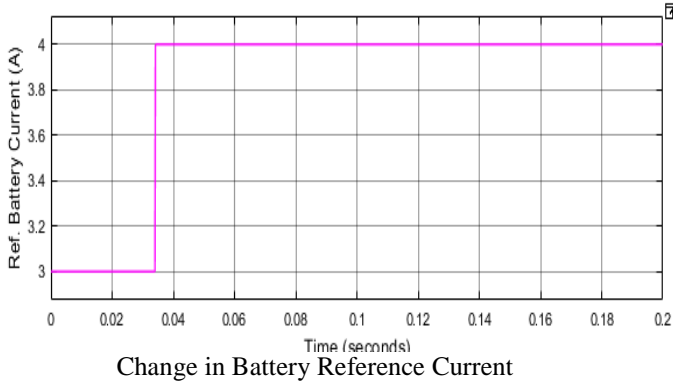
Reference Battery Current and Battery current during Discharging Model



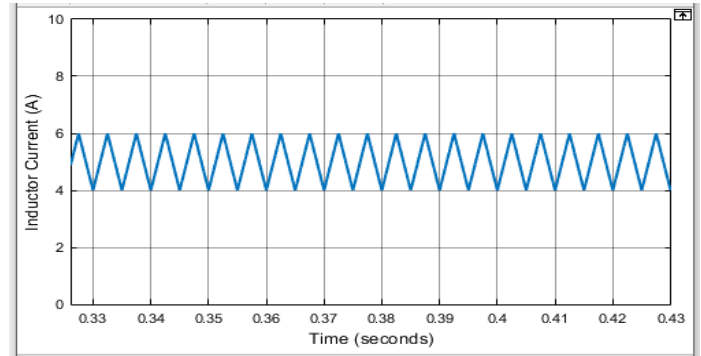
Inductor Current under discharging Mode



Simulation Model of the system

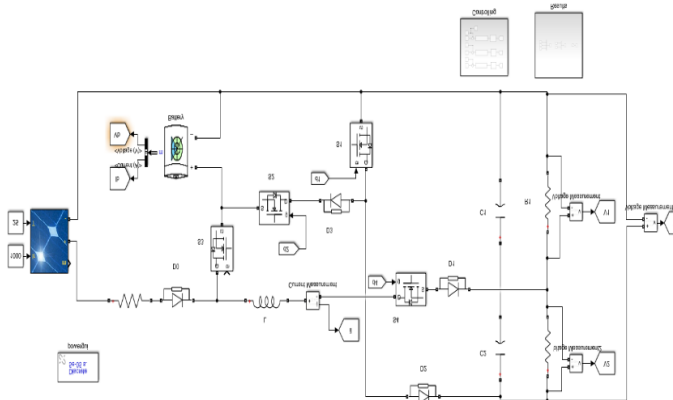


Change in Battery Reference Current

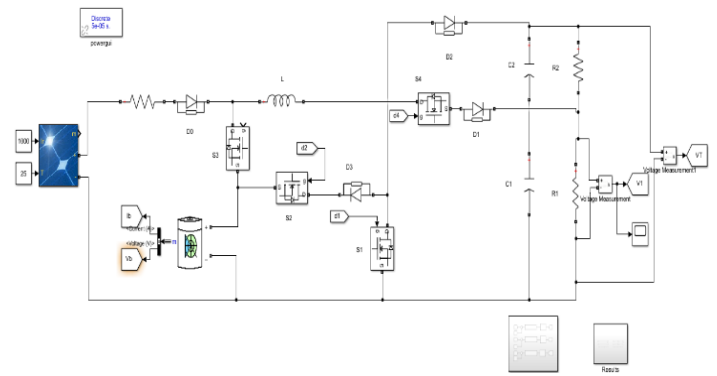


Inductor Current

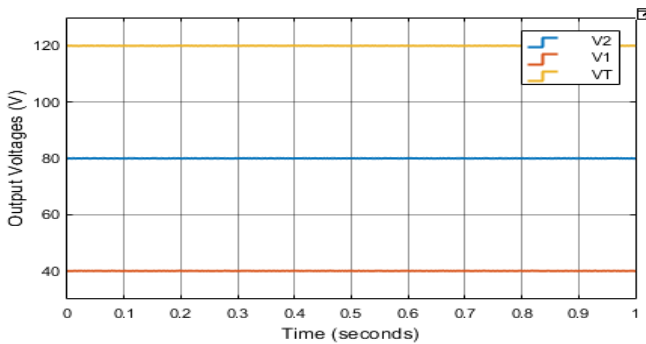
CHARGING MODE:



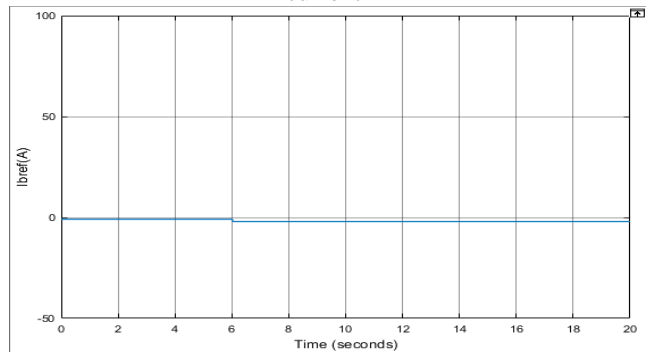
Simulation Model under Charging Mode



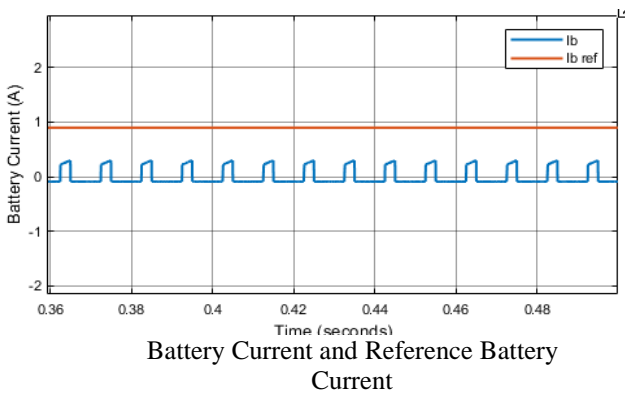
Simulation Model of variations in reference battery current



Output voltage under charging condition

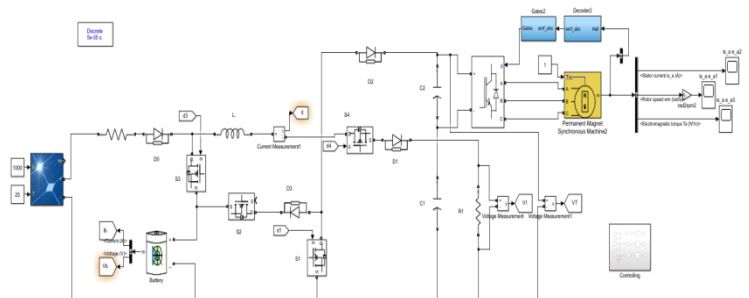


Variations in reference battery current

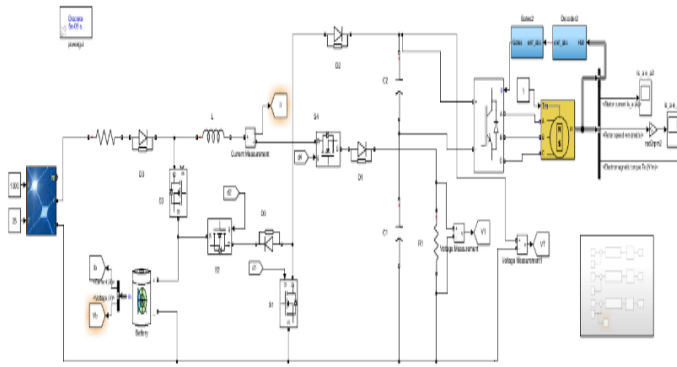


Battery Current and Reference Battery Current

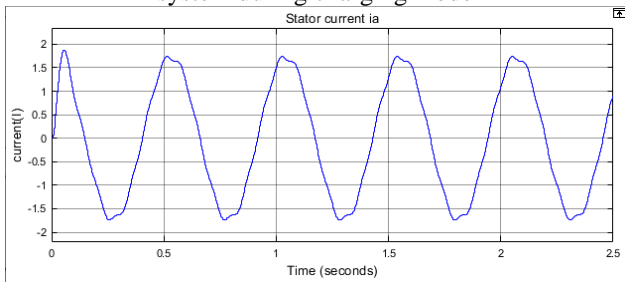
Electro-Magnetic Torque



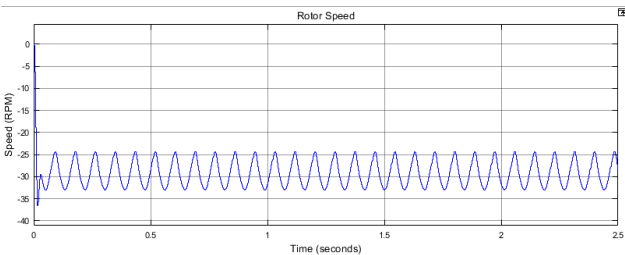
Simulation model of an EV when it is connected to an system during discharging mode



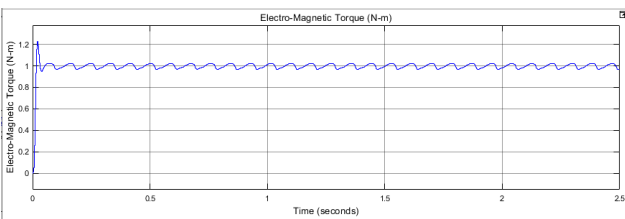
Simulation model of an EV when it is connected to an system during charging mode



Stator Current



Rotor Speed



Electro-Magnetic Torque

Simulation results validate that an STSMC can successfully control battery modes of charging and discharging of an EV system. Characteristic features of problems are:

COMPARISON:

Discharging Mode:

Battery Power Supply: Power is drawn by the motor from the battery via high stator current for torque creation and for driving the vehicle.
Motor Dynamics: Rotor speed and electro-magnetic torque increase characterize the motor energetic dynamics and the battery power conversion process to mechanical energy for traction.
Inductor Current: The most important parameter in the

efficient supply of the energy from the motor battery.

Charging

Mode:

Motor Activity: The motor is less active, maybe performing energy regenerating or regenerative braking with a lower stator current.
Rotor Speed and Torque: Rotor speed is low or idling and electro-magnetic torque is zero or less than during charging.

Inductor Function: The inductor regulates the amount of battery and not for overcharging.

Voltage and Current Characteristics:

Discharging: In the process of consuming energy, the voltage of the battery is reduced slowly.

Charging: In charging the battery, the voltage is raised to a higher voltage level.

Battery Current: The current exits the battery to the load, and back to the battery during the charging process. Very good reference current tracking is provided by the STSMC to ensure the best performance.

System Flexibility:

The STSMC control controls the switching from charging mode to discharging mode optimally with the best energy transmission and motor control in discharging and best and safe charging.

Generally, the system optimizes energy usage, improves driving economy, and protects battery life during driving and charging

VI. CONCLUSION

By effectively combining different energy sources, our new Super-Twisting Sliding Mode Control (STSMC) multi-port converter greatly boosts the performance of electric vehicle power systems. It does this by making everything more stable, cutting down on chattering, and enhancing the system's overall toughness. This controller creates a more reliable and efficient way to distribute energy. Both modeling and experiments show that it offers better energetic responses, less steady-state error, and excellent disturbance rejection when stacked up against traditional control methods. These findings indicate that this approach is perfect for electric vehicle applications, optimizing power management from renewable energy and battery storage.

REFERENCES

- [1] S.R. Khasim and C. Dhanamjayulu, "Selection parameters and synthesis of multi-input converters for electric vehicles: An overview," *Renew.Sustain.Energy Rev.*, vol.141,May 2021, Art no. 110804, doi: 10.1016/j.rser.2021.110804.
- [2] M. Zandi, A. Payman, J.P. Martin, S. Pierfederici, B. Davat, and F. Meibody-Tabar, "Energy management of a fuel cell/supercapacitor/battery power source for electric vehicular applications," *IEEE Trans. Veh. Technol.*, vol. 60, no.2, pp.433-443,Nov.2011.doi:10.1109/TVT.2010.2091433.
- [3] K. Suresh, C. Bharatiraja, N. Chellammal, M. Tariq, R. K.Chakraborty, M. J. Ryan, and B. Alamari,

- “A multifunctional non-isolated dual output converter for electric vehicle applications,” IEEE Access, vol. 9, 64445-64460, 2021.
- [4] A. Ajami, H. Ardi, and A. Farakhor, “A novel high step-up DC/DC converter based on integrating coupled inductor and switched capacitor techniques for renewable energy applications,” IEEE Trans. Power Electron., vol.30, no.8, pp. 4255-4263, Aug. 2015, doi:-10.1109/TPEL.2014.2360495.
- [5] S.R.Khasim and C.Dhanamjavulu, “Design and implementation of asymmetrical multilevel inverter with reduced components and low voltage stress,” IEEE Access, vol.10,pp.34953511,2022,doi:10.1109/ACCESS.2022.3140354.
- [6] C.Dhanamjavul,S.Padmanaban, V.K.Ramachandaramurth, J.B.Holm-Nielsen, and F.Blaabjerg, ”Design and implementation of multilevel inverters for electric vehicle,” IEEE ACCESS,vol.9,pp.317-388,2021
- [7] M. Dhananjaya, D. Ponuru, T.S. Babu, B.Aliafari, and H.H.Alhlou,” A new multi-output DC-DC converter for electric vehicle application,” IEEE ACCESS, vol.10,pp.19072-19082,2022.